Mineralogical Magazine, August 2016, Vol. 80(5), pp. 739–748

Mapping arsenopyrite alteration in a quartz vein-hosted gold deposit using microbeam analytical techniques

M. Gilligan[1], A. Costanzo[1,*], M. Feely[1], G. K. Rollinson[2], E. Timmins[3], T. Henry[4] and L. Morrison[1,5]

[1] Earth and Ocean Sciences, School of Natural Sciences, National University of Ireland, Galway, Ireland
[2] Camborne School of Mines, School of Engineering, Mathematics and Physical Sciences, University of Exeter, Cornwall Campus, Penryn, Cornwall TR10 9FE, UK
[3] National Centre for Biomedical Engineering Science, National University of Ireland, Galway, Ireland
[4] Earth and Ocean Sciences, School of Natural Sciences, National University of Ireland, Galway, Ireland
[5] Ryan Institute, National University of Ireland, Galway, Ireland

[*Received 23 February 2015; Accepted 30 June 2015; Associate Editor: Martin Lee*]

ABSTRACT

An unworked quartz vein-hosted gold deposit occurs in the Clew bay area of County Mayo, western Ireland. The veins are late-Caledonian in age and transect greenschist-facies poly-deformed Silurian quartzites. The veins contain disseminated arsenopyrite that may be a primary mineral source for elevated levels of arsenic (As) found in groundwater samples recovered from wells related spatially to the gold deposit. Levels from 5 to 188 μg/L (significantly above the 7.5 μg/L threshold for safe drinking water) have been detected. A series of element distribution maps using a scanning electron microscope (Hitachi model S-4700) linked to an energy-dispersive spectrometer (INCA® Oxford Instruments) and mineral distribution maps generated by QEMSCAN® (Quantitative Evaluation of Minerals by Scanning electron microscopy) were used to map the distribution of the primary arsenopyrite and related secondary As-bearing phases. Laser Raman microspectroscopy was used to identify the secondary As-bearing phases. 'Island weathering' of primary arsenopyrite together with hydrated pseudomorphs of arseniosiderite, pharmacosiderite and scorodite after arsenopyrite are recorded. Circulating groundwater hydrates the primary arsenopyrite, providing the release mechanism that forms the secondary As-bearing phases that occur as microfracture infills together with muscovite and biotite. The textural relationships between the primary and secondary As minerals indicate their potential as mineral sources of As that could enter transport pathways leading to its release into groundwater.

Keywords: arsenopyrite, gold deposit, Croagh Patrick.

Introduction

Routine sampling of groundwater in the study area, by local authority officials, revealed elevated arsenic levels in a number of wells. An Environmental Protection Agency (EPA)-funded study was undertaken to determine the source of the arsenic and to establish how it was being moved in the groundwater. The work presented here is part of that larger study. The results of a mineralogical study of auriferous quartz vein-hosted As-bearing minerals are presented here. The hydrogeological aspects of the larger study will be addressed in separate work.

The presence of arsenopyrite, pyrite and rare niccolite, in the quartz vein-hosted gold deposit, has been recorded by Aherne *et al.* (1992). Nesbitt *et al.* (1995) showed that oxidized arsenopyrite produces significant abundances of As^{3+} and As^{5+} on, or near, the surface of the mineral, thus facilitating rapid and selective leaching of arsenites (AsO_3^{3-}) and arsenates (AsO_4^{3-}). Arsenites are toxic to biota (Flora, 2015) and can be mobilized in groundwater where flow regimes are related spatially to arsenopyrite-bearing bedrock or to

* E-mail: alessandra.costanzo@nuigalway.ie
DOI: 10.1180/minmag.2016.080.019

arsenopyrite-bearing gangue spoil heaps (Henry, 2014; Basu and Schreiber, 2013; Smedley and Kinniburgh, 2002). Total arsenic levels in the groundwater samples recovered from wells related spatially to these auriferous quartz veins range in concentration from ~5 to 188 µg/L of which 30% are above the groundwater threshold value (GTV) of 7.5 µg/L for safe drinking water in Ireland (European Communities Environmental Objectives (Groundwater) Regulations (2010); Gilligan *et al.*, 2013).

The objective of this study was to apply a suite of microscopic and spectroscopic analytical techniques to map the distribution of As and associated elements (e.g. Fe and S), to identify and characterize the *in situ* alteration patterns within arsenopyrite, and to identify the secondary As minerals present in the gold-bearing quartz vein. The significance of the resulting element and mineral distribution maps is discussed. A model for alteration of primary arsenopyrite and the formation of secondary As-bearing minerals is proposed. Release of As at the microscopic scale and possible inferences for As release into groundwater are the focus of this model.

Geological and hydrogeological setting of the quartz vein-hosted gold deposit.

The auriferous quartz veins in the study area range in thickness from ~0.2 to 2.0 m and constitute the unworked Croagh Patrick gold deposit (250,000 t of 10 g/t Au), County Mayo, west of Ireland (Aherne *et al.*, 1992, Wilkinson and Johnston, 1996). The veins are related spatially to shear zones that crosscut polydeformed greenschist-facies Silurian quartzites. The quartz veins formed during the late-Caledonian tectonism (Wilkinson and Johnston, 1996; Johnston and McCaffrey, 1996). Cambro-Ordovician ophiolites and metasediments and Lower Carboniferous limestones occur to the north along the south shore of Clew Bay (Fig. 1*a*).

Core samples from eight gold-exploration drillholes, from the mid-1980s exploration project (Aherne *et al.*, 1992), were examined in the Geological Survey of Ireland's (GSI) core store in Dublin. Quartz vein samples containing visible arsenopyrite were examined and the most suitable quartz vein sample (13A) was selected for this study. The sample is from the Kilgeever DH2879-11 borehole core, at a depth of 16.46 m (see Fig. 1*a* for location of the drill hole) and contains several visible microfractures that contain arsenopyrite.

Groundwater flows in the study area are controlled topographically, with flow from the flanks of Croagh Patrick to the lowlands to the north and west (Fig. 1*b*). The entire area is classed by the GSI as a 'Poor Aquifer (Pl)' which is generally unproductive except for local zones. Surface drainage is dominant but shallow groundwater discharges, frequently mediated by faults, fractures and weathered ground, are present.

A number of the wells that are situated downslope and hydraulically down-gradient of the arsenic-bearing auriferous quartz veins are located on the EW trending Silurian quartzite ridge (Fig. 1*b*). Samples recovered from these wells showed elevated levels of As.

Analytical methods

Mineralogical and textural studies of the sample used three microbeam analytical techniques to identify the primary and secondary As-bearing phases and to map the spatial distribution of key elements (e.g. As, S and Fe). The following analytical techniques were utilized: scanning electron microscopy with energy-dispersive spectroscopy (SEM-EDS); QEMSCAN® (quantitative evaluation of minerals by scanning electron microscopy); and laser Raman microspectroscopy (LRM).

The SEM-EDS analysis was carried out using a Hitachi SEM model S-4700 with EDS (INCA® Oxford Instruments, UK) at the National University of Ireland Galway (NUIG). The EDS generated element spatial distribution maps of As, Fe, S, Si and Ca in the sample.

The automated system QEMSCAN® was developed originally to provide quantitative mineralogical data for the mining sector (Gottlieb *et al.*, 2000; Goodall *et al.*, 2005) but is now used to study a range of materials including rocks and minerals in a range of geological settings (Pirrie and Rollinson, 2011; Knappett *et al.*, 2011). This innovative technology uses automated scanning electron microscopy linked to an energy-dispersive spectrometer (SEM-EDS) to map the mineralogy of rocks. A polished thin section was prepared for QEMSCAN® analysis at the Camborne School of Mines, UK. The instrument consists of a QEMSCAN® 4300 system which utilizes a Zeiss EVO 50 series SEM consisting of four light-element Bruker Silicon Drift Droplet Energy-Dispersive X-ray Spectrometers equipped with a back-scattered electron (BSE) detector.

https://doi.org/10.1180/minmag.2016.080.019 Published online by Cambridge University Press

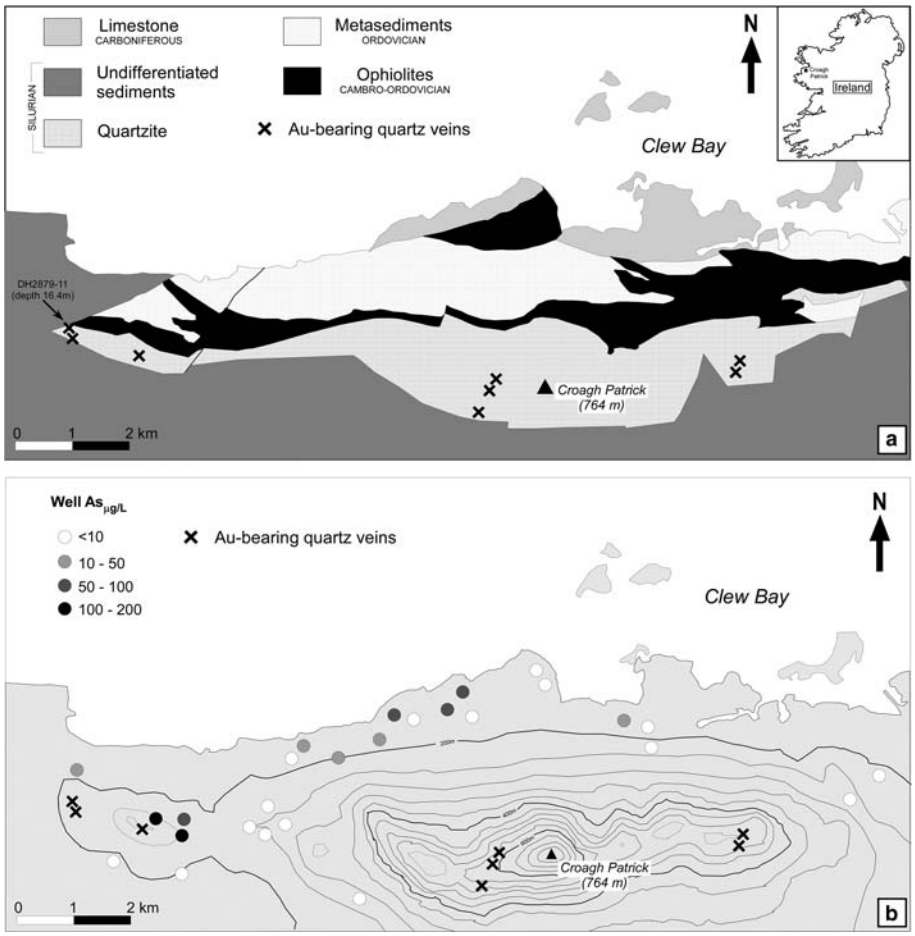

FIG. 1. (*a*) Simplified geological map of the southern shore, Clew Bay, County Mayo, Ireland. The spatial distribution of the main lithological units is shown together with the locations of the main auriferous quartz veins. (*b*) Map showing the spatial relationships between the main arsenic-bearing auriferous quartz veins, the topographic highs and the groundwater wells in the study area (after Gilligan *et al.*, 2010, 2013).

Thin-section analysis by QEMSCAN® uses a combination of back-scattered electrons and X-rays to examine the sample. An electron beam is rastered across the sample surface producing a BSE image and X-rays at pre-defined point spacing. At each analysis point the resultant chemical X-ray spectrum is compared with a database of >750 known minerals or compounds and assigned to the most appropriate one. The whole process is computer controlled using inbuilt iMeasure software. The data are then processed to produce a simplified mineral/phase list using iDiscover software, which includes database development as required. Once complete, data outputs include modal mineralogy and false-colour mineral maps.

Polished thin sections of quartz veins were used to identify the arsenopyrite alteration phases using a Horiba LabRam II Raman spectrometer at NUIG. The instrument is equipped with a 600 groove per mm diffraction grating, confocal optics, a Peltier-cooled CCD detector (255 by 1024 pixel array at –67°C) and an Olympus BX41 microscope arranged in 180° back-scatter geometry. Sample excitation was performed using a Ventus diode-pumped, continuous wavelength, 532 nm laser with a maximum power output of 50 mW. Raman

https://doi.org/10.1180/minmag.2016.080.019 Published online by Cambridge University Press

analyses were carried out using a 100 × microscope objective resulting in a laser spot size of ~2 μm. Excitation power at the sample ranged typically between 10 and 20 mW.

Results

A digitally scanned image of sample 13A is presented, side-by-side, with a QEMSCAN® generated false-colour mineral distribution map in Figs 2*a* and *b*. The entire thin section (measuring 23 mm × 26 mm) of the quartz vein (Fig. 2*a*) was analysed using the Fieldscan measurement mode which used a 10 μm X-ray pixel spacing (Fig. 2*b*) and a smaller area (2 mm^2) at a higher resolution of 1 μm X-ray pixel spacing (Fig. 4*a*). Both scan modes provided excellent modal mineralogy and textural detail. Clear textural and mineralogical correlations can be made between the polished thin section in Fig 2*a* and the QEMSCAN® image in Fig. 2*b*. Braided micrometre-scale fractures, variously containing arsenopyrite, Fe-Ca-As and Fe-K-As phases, muscovite, biotite and accessory pyrite, transect the host quartz vein.

The results of the SEM-EDS analysis are combined with mineral maps in Figs 3 and 4. Specifically, element spatial distribution maps for silicon (Si), arsenic (As), iron (Fe), calcium (Ca) and sulfur (S) together with QEMSCAN® and SEM images are presented in Figs 3 and 4 (*a* to *g*). The EDS-generated element distribution maps show that the microfractures contain As and Fe that was derived from chemically altered arsenopyrite. Furthermore, the relatively unaltered cores of arsenopyrite are rimmed by Ca (Figs 3*d* and 4*d*) which is also present, along with the As and Fe, in the microfractures. The relatively unaltered cores of the arsenopyrite are marked by the presence of S (Figs 3*f* and 4*f*). Furthermore, Ca together with As and Fe, can be mapped continuously from the arsenopyrite crystals into the microfractures. The Fe and Ca maps provide unequivocal proof that the arsenopyrite has been subjected to chemical weathering. The texture displayed by the relics of arsenopyrite is similar to the well-documented 'island weathering', an alteration texture displayed commonly by the mineral olivine when it is hydrated (Deer *et al.*, 2013). This causes the release of Fe which forms micro-channels of iron oxide with the synchronous formation of the hydrated Mg-bearing silicate serpentine (Deer *et al.*, 2013).

Figure 4*a* clearly highlights the island weathering texture and identifies the presence of

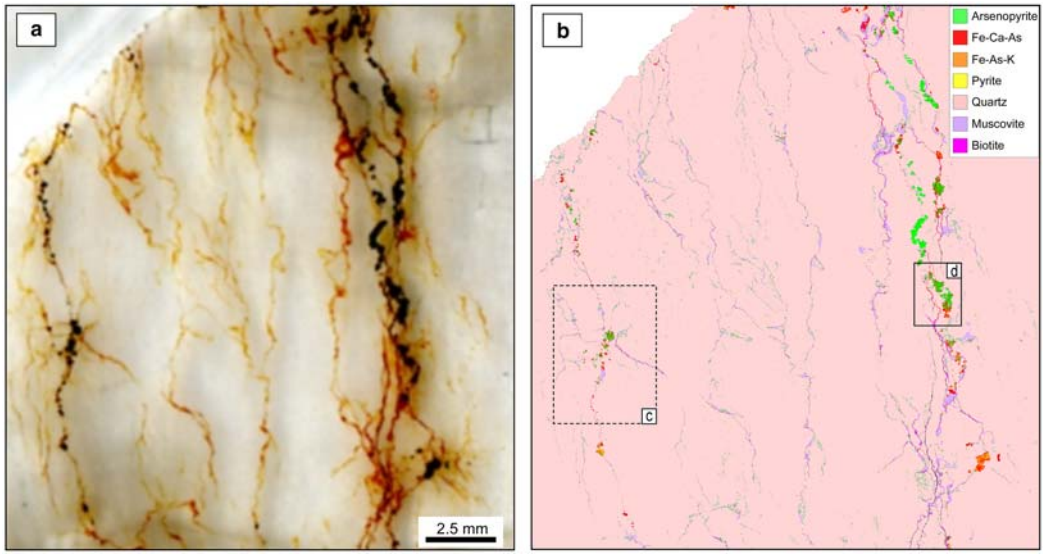

FIG. 2. (*a*) A digitally scanned image of a polished thin section of sample 13A (Kilgeever DH2879-11, sample depth 16.4 m). (*b*) QEMSCAN® generated false-colour mineral distribution map of the entire thin section shown in (*a*). This is the lower resolution map (see text). Microfractures on the right and left contain opaque arsenopyrite (green). Alteration of arsenopyrite to a dominant Ca-Fe-As phase (red) and a very restricted occurrence of a K-Fe-As phase (orange) are displayed. The microfractures also contain the phyllosilicates biotite (fuchsia) and muscovite (purple). The areas outlined (*c* and *d*) in Fig. 2*b* were chosen for SEM-EDS and LRM analyses (see Figs 3, 4 and 5).

https://doi.org/10.1180/minmag.2016.080.019 Published online by Cambridge University Press

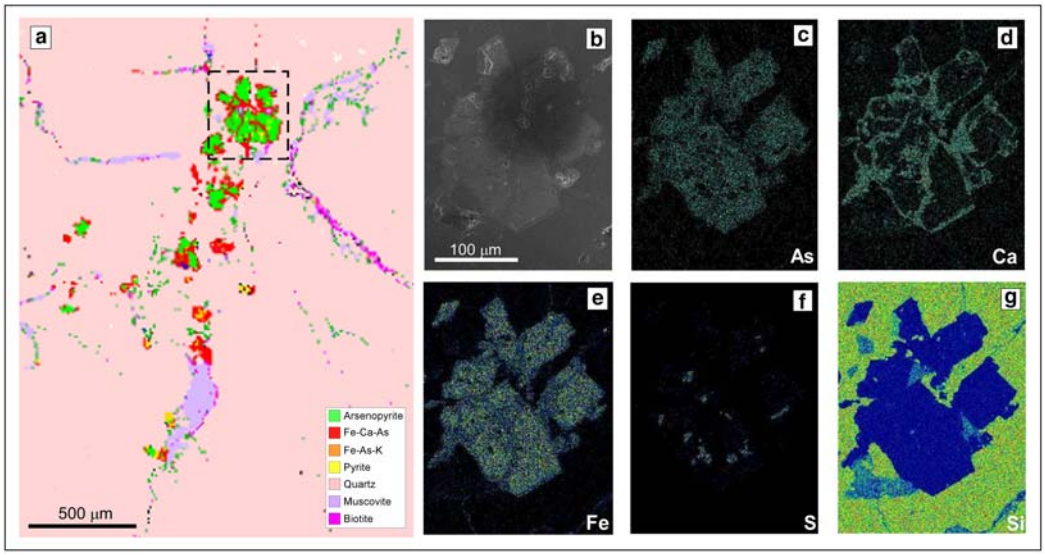

FIG. 3. (*a*) QEMSCAN® mineral distribution map of location *c* in Fig. 2*b*. Note that this is an enlargement of the lower resolution mineral map in Fig 2*b*. (*b* to *g*) SEM image and EDS element (As, Ca, Fe, S and Si) distribution maps of area outlined in (3*a*) above (image and maps rotated slightly clockwise with respect to 3*a*).

Fe-Ca-As and Fe-K-As phases in the arsenopyrite alteration rims and its intra- and inter-crystalline crosscutting channels. Furthermore, these phases along with biotite and muscovite are clearly visible in the microfractures. In the arrowed portion of the map (Fig. 4*a* – lower right) it is also evident that total replacement of the arsenopyrite (green) has led to the formation of composite pseudomorphs of

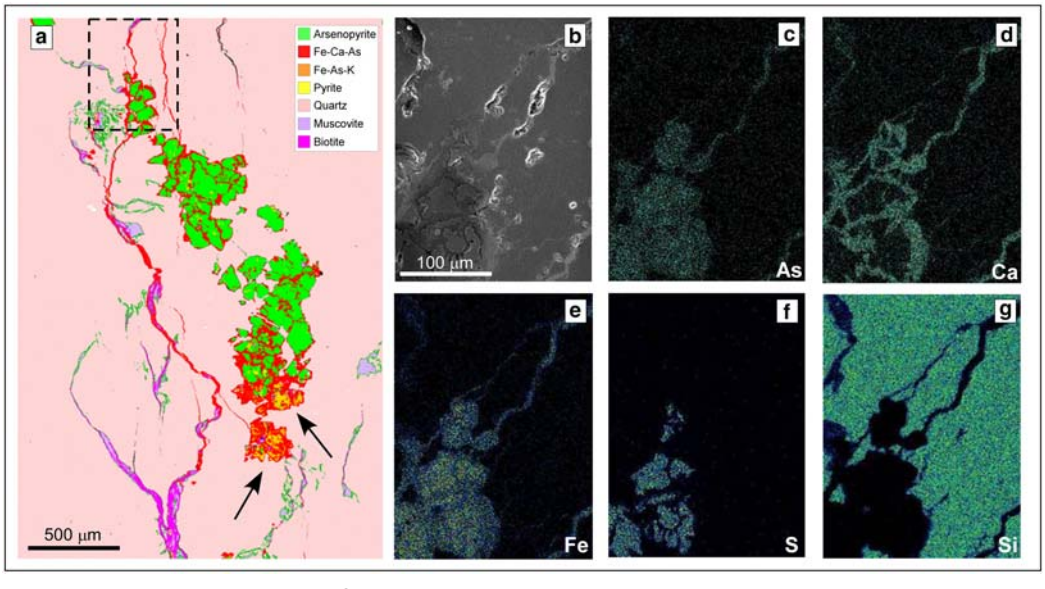

FIG. 4. (*a*) High resolution QEMSCAN® mineral map of location *d* in Fig. 2*b*. (*b* to *g*) SEM image (*b*) and EDS element distribution maps for the area outlined in (*a*) (image and maps rotated slightly clockwise with respect to 4*a*).

https://doi.org/10.1180/minmag.2016.080.019 Published online by Cambridge University Press

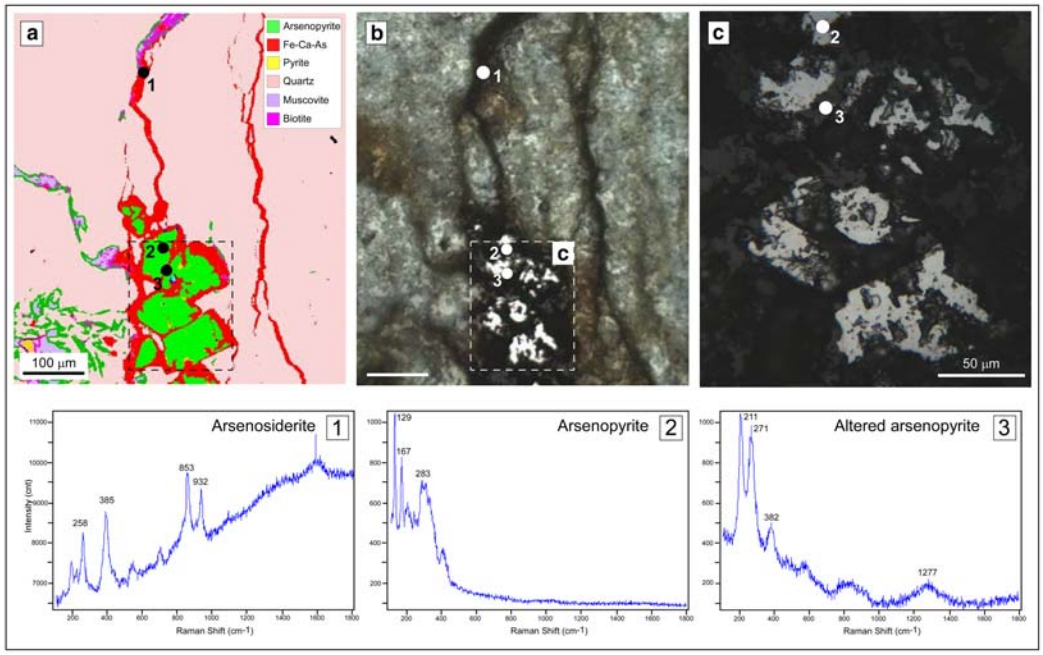

FIG. 5. (*a*) QEMSCAN® false-colour mineralogy map (high resolution – 1 µm pixel spacing) used to target phases for LRM; the laser spot analyses are numbered 1 to 3 on the map and correlate with the numbers in (*b*) and (*c*). Note that this is an enlargement of the lower resolution mineral map (outlined area) in Fig. 4*a*. (*b*) Transmitted ordinary light photomicrograph of the thin-section area in (*a*) above showing the location of LRM spot analysis 1. (*c*) Magnified transmitted ordinary light image of area (*c*) in image (*b*) above. LRM analytical spots 2 and 3 are shown. The laser Raman spectra 1, 2 and 3 correlate with the analytical spots in (*a*), (*b*) and (*c*) above.

Fe-Ca-As (red) and Fe-K-As (orange) phases. To the left of this area a microfracture occurs containing the Fe-Ca-As phase along with biotite (fuchsia) and muscovite (purple). This microfracture continues to the top of the thin section where it links with altered arsenopyrite.

Laser Raman microscopy was used to identify the secondary As-bearing phases mapped by QEMSCAN®. The high-resolution map was used to target the phases of interest in the thin section (Fig. 5*a*). Prior to LRM analyses, microscopic examination of the area, in transmitted ordinary light, (Figs 5*b* and 5*c*) confirmed the presence of three phases. The first phase has a dark grey colour in transmitted light and appears red (Figs 5*a* and 5*b* (spot 1). This infills the microfractures at the centre and right hand side of the map and also mantles the arsenopyrite (Fig. 5*a*). The second phase has a light grey colour in transmitted light (Fig. 5*c*; spot 2) and it corresponds to a green area in the QEMSCAN® map (Fig. 5*a*; spot 2). Finally, the third phase is darker grey and rims the lighter grey phase (Fig. 5*c*; spot 3).

The laser Raman spectrum for spot 1 (Fig. 5, Raman spectrum 1) correlates well with that produced by arseniosiderite ($Ca_2Fe^{3+}_3(AsO_4)_3O_2{\cdot}3H_2O$) which has its main Raman peaks at ~250, ~389, ~852 and ~927 cm^{-1} (Gomez *et al.*, 2010).

The laser Raman spectrum for spot 2 confirms the presence of arsenopyrite which has Raman peaks at 133, 170 and 281 cm^{-1} (Filippi *et al.*, 2009). The laser Raman peaks for spot 3 located at the margin of arsenopyrite, does not match recently published Raman arsenopyrite spectra (Filippi *et al.,* 2009) but does correlate well with a much earlier spectrum (Mernagh and Trudu, 1993). This is probably due to arsenopyrite alteration. Scorodite ($FeAsO_4{\cdot}2H_2O$) was also recorded in the quartz vein during this study. Its Raman spectrum displays strong peaks at 801 and 888 cm^{-1} (Bossy *et al.*, 2010; Das and Hendry, 2011). Finally, Fig. 4*a* records the presence of a K-Fe-As phase (orange colour and arrowed in the mineral map); this element association indicates that this phase is

https://doi.org/10.1180/minmag.2016.080.019 Published online by Cambridge University Press

the secondary arsenate phase pharmacosiderite ($K[Fe_4(OH)_4(AsO_4)_3]\cdot 6.5H_2O$) which commonly occurs alongside arseniosiderite. Arseniosiderite, scorodite and pharmacosiderite are common secondary minerals after arsenopyrite (Bossy *et al.*, 2010; Drahota and Filippi, 2009).

Discussion

The alteration of arsenopyrite

Foley and Ayuso (2008) identified mineral reaction pathways involved in the release of As to the groundwater of coastal Maine. In general, oxidation of primary arsenopyrite is thought to be among the processes responsible for the initial release of As from bedrock minerals such as arsenopyrite (Utsunomiya *et. al.,* 2003; Lipfert, 2006; Foley and Ayuso, 2008). Groundwater studies suggest either a single mineral (e.g. arsenopyrite) or a restricted suite of As-bearing minerals as the dominant source of As in the groundwater environments (Henry, 2014; Smedley and Kinniburgh, 2002). The As released from its primary host mineral then becomes sequestered in secondary As-bearing minerals including arseniosiderite, pharmacosiderite and scorodite (Foley and Ayuso, 2008). These can behave as secondary As-reservoirs and they may subsequently be mobilized in groundwater. Reductive dissolution may account for the ultimate release of As and Fe into groundwater (Foley and Ayuso, 2008).

This study shows that arsenopyrite is the primary As-bearing phase in the quartz vein. Hydration by circulating groundwaters is the most probable mechanism for the release of As from the arsenopyrite and the subsequent formation of arseniosiderite, scorodite and pharmacosiderite. Foley and Ayuso (2008), in considering models for sources and transport pathways of As in Maine's groundwater, show that oxidative dissolution of primary arsenopyrite leads to the formation of secondary As minerals such as Ca-arsenates. The recognition of hydrated secondary arseniosiderite, scorodite and pharmacosiderite in this study reflects the release of As and indeed Fe and S from its primary mineral source. The secondary minerals (arseniosiderite, scorodite and pharmacosiderite) can act as intermediate As reservoirs that may eventually form part of the chain of reactions that ultimately release As into groundwater (see Foley and Ayuso, 2008). Primary arsenopyrite and three secondary arsenates (arseniosiderite, pharmacosiderite and scorodite) were recorded during this study.

Unstable chemical parameters of the groundwaters.

Groundwater samples were recovered for full chemical analysis from a number of wells in the study area and these results will be the focus of further publications. Unstable parameters were recorded as the samples were recovered, including Eh and pH. The Eh and pH bivariate plots for the samples are presented in Fig. 6, and suggest that groundwater conditions are reducing (alkaline) in character (Figs 6*a* and *b*). The samples all plot within the shallow groundwater envelope, which fits with the aquifer classification and the hydrogeological properties of the bedrock. In addition, the Eh-pH values essentially straddle the boundary of, and plot within, the $HAsO_4^{2-}$ field. This indicates that As is present in solution primarily as As(V) (Smedley and Kinniburgh, 2002).

Total As and Fe abundances in the groundwater wells display large variability with As ranging from ~6 to 200 µg/L (mean = 57 µg/L; $n = 26$) and Fe from 21 to 6580 µg/L (mean = 828 µg/L; $n = 21$). Changes in groundwater pH can promote adsorption or desorption of arsenic (Hinkle and Polette, 1999). Because solid-phase diagenesis (water-rock interaction) typically consumes H^+ (Stumm and Morgan, 1996), the pH of groundwater tends to increase with residence time, which, in turn, increases along groundwater flow paths. Because iron-oxide surfaces can hold large amounts of adsorbed arsenate, geochemical evolution of groundwater to high (alkaline) pH can induce desorption of arsenic sufficient to result in elevated levels in groundwater (Hinkle and Polette, 1999; Robertson, 1989). The pH values are typical for Irish groundwaters and in this case the range of pH is relatively narrow (between 6 and 8) and the groundwater residence time is very short. While there are established strong correlations between Fe and As occurrences associated with the conditions described above (Smedley and Kinniburgh, 2002) results of studies in Ireland are less conclusive (Henry, 2014). A bivariate plot of groundwater As and Fe pairs from the study area (Fig. 7) shows that no correlation exists between total As and Fe. It is probable that the reducing (slightly alkaline) character of the groundwaters facilitates desorption of As, which is reflected in elevated levels in a number of the sampled groundwaters. Detailed

https://doi.org/10.1180/minmag.2016.080.019 Published online by Cambridge University Press

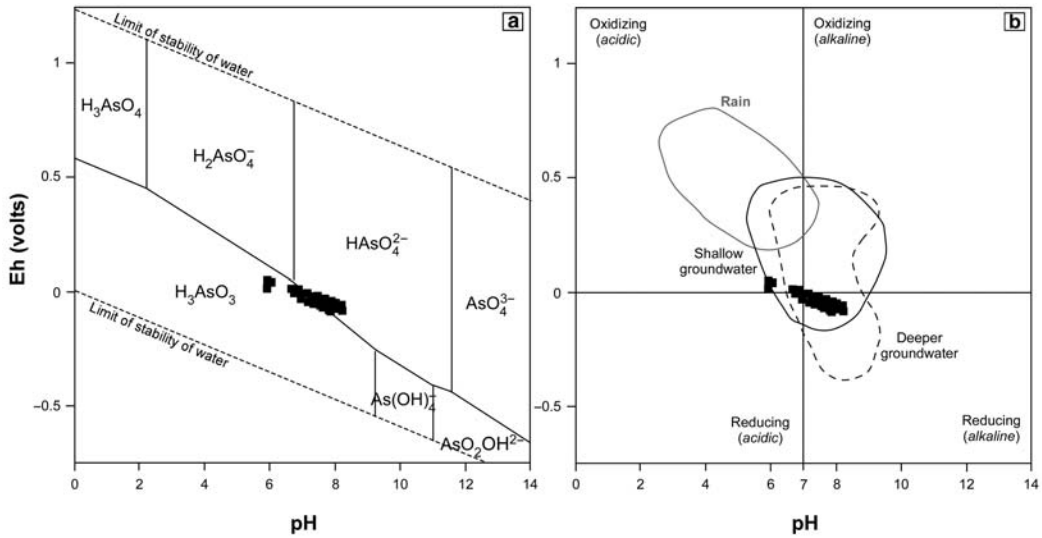

FIG. 6. Eh and pH bivariate plots for the analysed groundwater wells. (*a*) The majority of the data plot within the $HAsO_4^{2-}$ field. The diagram also includes upper and lower, stability limits for water, represented by the oxygen (oxidizing agent) and hydrogen (reducing agent) reactions. (*b*) The four regions depicted in the diagram correspond to oxidizing (acidic), oxidizing (alkaline), reducing (acidic) and reducing (alkaline) environments. Fields for rain water, shallow and deeper groundwater are also shown. Number of analyses = 37.

chemical analyses of all of the groundwater samples has been completed and will be reported in subsequent publications.

Summary and conclusions

A series of elemental distribution maps using SEM-EDS- and QEMSCAN®-generated mineral distribution maps display the spatial distribution of arsenic and As-bearing phases in auriferous quartz veins. The element distribution maps highlight the alteration of arsenopyrite and subsequent channelling of released As and Fe into fractures. The alteration of the primary arsenopyrite has led to the weathering of primary arsenopyrite and to the formation of pseudomorphs of arseniosiderite and pharmacosiderite after arsenopyrite. These

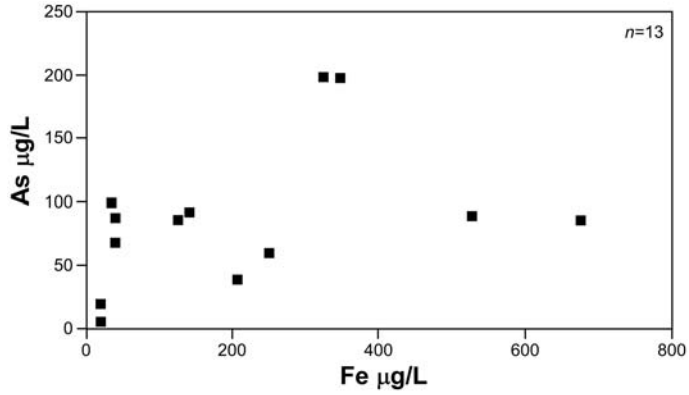

FIG. 7. Bivariate plot of groundwater As and Fe pairs (µg/L) highlighting a lack of correlation between As and Fe abundances.

https://doi.org/10.1180/minmag.2016.080.019 Published online by Cambridge University Press

secondary minerals are at least intermediate As phases that form part of the mineral sources and transport pathways for arsenic release into the environment.

Acknowledgements

The authors wish to acknowledge funding from the Environmental Protection Agency (EPA) under the STRIVE programme 2007-2013 (project No. 2008-PHD-EH-2) and from the Geofluids Research Laboratory, NUI, Galway.

References

Aherne, S., Reynolds, N.A. and Burke, D. (1992) Gold mineralization in the Silurian and Ordovician of South Mayo. Pp. 39–49 in: *The Irish Minerals Industry 1980–1990* (A.A. Bowden, editor). Irish Association for Economic Geology, Dublin.

Basu, A. and Schreiber, M.E. (2013) Arsenic release from arsenopyrite weathering: Insights from sequential extraction and microscopic studies. *Journal of Hazardous Materials*, **262**, 896–904.

Bossy, A., Grosbois, C., Beauchemin, S., Courtin-Nomade, A., Hendershot, W. and Bril, H. (2010) Alteration of As-bearing phases in a small watershed located on a high grade arsenic-geochemical anomaly (French Massif Central). *Applied Geochemistry*, **25**, 1889–1901.

Das, S. and Hendry, M.J. (2011) Application of Raman spectroscopy to identify iron minerals commonly found in mine wastes. *Chemical Geology*, **290**, 101–108.

Deer, W.A., Howie, R.A. and Zussman, J. (2013) *An Introduction to the Rock-forming Minerals.* 3rd edition. Mineralogical Society of Great Britain and Ireland, London, 498 pp.

Drahota, P. and Filippi, M. (2009) Secondary arsenic minerals in the environment: A review. *Environment International*, **35**, 1243–1255.

European Communities Environmental Objectives (Groundwater) Regulations (2010) Statutory Instruments (SI) No 9 of 2010. Government of Ireland.

Filippi, M., Machovic, V., Drahota, P. and Bohmova, V. (2009) Raman microspectroscopy as a valuable additional method to X-ray diffraction and electron microscope/microprobe analysis in the study of iron arsenates in environmental samples. *Applied Spectroscopy*, **63**, 621–626.

Flora, S.J.S. (2015) Arsenic: chemistry, occurrence, and exposure. Chapter 1 in: *Handbook of Arsenic Toxicology* (S.J.S. Flora, editor). Elsevier, 723 pp.

Foley, N.K. and Ayuso, R.A. (2008) Mineral sources and transport pathways for arsenic release in a coastal watershed, USA. *Geochemistry: Exploration, Environment, Analysis*, **8**, 59–75.

Gilligan, M., Feely, M., Higgins, T., Henry, T., Zhang, C. and Morrison, L. (2010) Elevated arsenic in grounwater from the western Irish Caledonides: evidence for cross atlantic correlations with high arsenic groundwater provenances along the Appalachian-Caledonian belt. *SEGH, Conference Schedule and Abstracts*, p 56 [Available from www.nuigalway.ie/segh2010/download/SEGH2010%20Book_of_Abstracts.pdf].

Gilligan, M., Feely, M., Henry, T., Higgins, T., Zhang, C., Timmins, E., Rollinson, G.K. and Morrison, L. (2013) *Spatial distribution of As in gold bearing quartz veins from a high As groundwater region in the Caledonides of Western Ireland*. GSA Abstracts with programs, **45**, No. 1, p. 46 [Available from https://gsa.confex.com/gsa/2013NE/webprogram/Paper216124.html].

Gomez, M.A., Becze, L., Blyth, R.I.R., Cutler, J.N. and Demopoulos, G.P. (2010) Molecular and structural investigation of yukonite (synthetic & natural) and its relation to arseniosiderite. *Geochimica et Cosmochimica Acta*, **74**, 5835–5851.

Goodall, W.R., Scales, P.J. and Butcher, A.R. (2005) The use of QEMSCAN and diagnostic leaching in the characterization of visible gold in complex ores. *Minerals Engineering*, **18**, 877–886.

Gottlieb, P., Wilkie, G., Sutherland, D., Ho-Tun, E., Suthers, S., Perera, K., Jenkins, B., Spencer, S., Butcher, A. and Rayner, J. (2000) Using quantitative electron microscopy for process mineralogy applications. *Journal of the Minerals Metals & Materials Society*, **52**, 24–25.

Henry, T. (2014) *An integrated approach to characterising the hydrogeology of the Tynagh Mine catchment, County Galway, Ireland*. Unpublished PhD Thesis, National University of Ireland Galway, Ireland [http://hdl.handle.net/10379/3976].

Hinkle, S.R. and Polette, D.J. (1999) Arsenic in Ground Water of the Willamette Basin, Oregon. *Department of the Interior U.S. Geological Survey. Water-Resources Investigations Report* 98–4205.

Johnston, J.D. and McCaffrey, K.J.W. (1996) Fractal geometries of vein systems and the variation of scaling relationships with mechanism. *Journal of Structural Geology*, **18**, 349–358.

Knappett, C., Pirrie, D., Power, M.R., Nikolakopoulou, I., Hilditch, J. and Rollinson, G.K. (2011) Mineralogical analysis and provenancing of ancient ceramics using automated SEM-EDS analysis (QEMSCAN®): a pilot study on LB I pottery from Akrotiri, Thera. *Journal of Archaeological Science*, **38**, 219–232.

Lipfert, G. (2006) *A geochemical, isotopic and petrologic study of a watershed with arsenic-enriched ground water in Northport, Maine*. PhD Thesis, University of Maine, Orono, USA.

https://doi.org/10.1180/minmag.2016.080.019 Published online by Cambridge University Press

Mernagh, T.P. and Trudu, A.G. (1993) A laser Raman microprobe study of some geologically important sulphide minerals. *Chemical Geology*, **103**, 113–127.

Nesbitt, H.W., Muir, I.J. and Prarr, A.R. (1995) Oxidation of arsenopyrite by air and air-saturated, distilled water, and implications for mechanism of oxidation. *Geochimica et Cosmochimica Acta*, **59**, 1773–1786.

Pirrie, D. and Rollinson, G.K. (2011) Unlocking the applications of automated mineral analysis. *Geology Today*, **27**, 235–244.

Robertson, F.N. (1989) Arsenic in ground-water under oxidizing conditions, south-west United States. *Environmental Geochemistry and Health*, **11**, 171–186.

Smedley, P.L. and Kinniburgh, D.G. (2002) A review of the source, behaviour and distribution of arsenic in natural waters. *Applied Geochemistry*, **17**, 517–568.

Stumm, W. and Morgan, J.J. (1996) Aquatic Chemistry, *Chemical Equilibria and Rates in Natural Waters.* 3rd edition. John Wiley & Sons, Inc., New York, 1022 pp.

Wilkinson, J.J. and Johnston, J.D. (1996) Pressure fluctuations, phase separation, and gold precipitation during seismic fracture propagation. *Geology*, **24**, 395–398.

Utsunomiya, S., Peters, S.C., Blum, J.D. and Ewing, R.C. (2003) Nanoscale mineralogy of arsenic in a region of New Hampshire with elevated As concentration in the groundwater. *American Mineralogist*, **88**, 1844–1852.

https://doi.org/10.1180/minmag.2016.080.019 Published online by Cambridge University Press